Annals of Nuclear Energy 124 (2019) 179–186

Contents lists available at ScienceDirect

Annals of Nuclear Energy

journal homepage: www.elsevier.com/locate/anucene

A numerical simulation of single bubble growth in subcooled boiling water

Ning Cheng, Yun Guo, Changhong Peng *

School of Nuclear Science and Technology, University of Science and Technology of China, Hefei, Anhui Province 230026, China

ARTICLE INFO

Article history:
Received 3 December 2017
Received in revised form 10 September 2018
Accepted 1 October 2018
Available online 10 October 2018

Keywords:
Subcooled boiling
Single bubble growth
Numerical simulation
VOF method

ABSTRACT

Water-cooling blanket is closely related to system safety in future fusion reactor for it can cooling down the reactor. The process of cooling in water-cooling blanket may involve bubble generation under subcooled boiling condition. Although many researchers have investigated bubble generation numerically, the details of bubble generation in subcooled boiling remain unclear. In this paper a two-dimensional bubble growth simulation under subcooled nucleate boiling condition has been conducted using VOF (Volume of Fluid) method in ANSYS FLUENT. A phase change model was adopted by adding extra mass source term and energy source term to the Navier-Stokes equations in the cells adjacent to vapor-liquid interface. The variations of bubble contour before bubble departure, temperature fields, velocity fields and contribution of heat flux from superheated layer and subcooled fluid can be obtained by simulation. The results were compared with existing datum of visual experiment in previous literature to verify the validity of the simulation.

1. Introduction

While the subcooled coolant flows through a superheated channel in water-cooling blanket during the cooling process in fusion reactor, the one-phase flow will transfer into two-phase flow at the ONB (Onset of Nucleate Boiling) point where the wall temperature exceeds the saturation temperature sufficiently. The generation of bubbles is a basic problem in ONB research, although bubbles can improve heat transfer capability significantly, they can also lead to critical-thermal hydraulic events such as CHF (Critical Heat Flux) and OFI (Onset of Fluid Instability), thus affecting the safety of reactor.

To figure out the mechanism of bubble growth in subcooled nucleate boiling, many efforts have been done in the last few decades. Numerical simulation is one of the most important means to investigate two phase flow problem and the VOF method is a popular interface capturing methods adopted by many researchers. Welch and Wilson (2000) calculated mass transfer rate directly from the heat flux at the liquid–vapor interface coupled with VOF, but it may show a deformed bubble shape due to the numerical error in phase change model despite good mass conservation. Hardt and Wondra (2008) proposed a phase-change model based on VOF. The mass transfer rate estimated from the evaporation heat transfer coefficient is artificially shifted to liquid side or vapor side for condensation and evaporation to avoid the deformation of the interface. Tomar et al. (2005) developed a phase change model based on coupled Level Set and VOF method. There are little research about this method in literature although it's reported mass conservative and interface topologies accurate.

Most of previous works simulated bubble growth under saturated boiling condition, simulation of bubble growth in subcooled boiling is more difficult while there are few papers about it. In this paper the VOF method in ANSYS FLUENT was used to simulate bubble growth process in subcooled boiling under two-dimensional condition. The mass flow was calculated by a phase change model proposed by Lee (Lee and Veziroglu, 1980) according to local temperature, and was artificially moved to the cells adjacent to vapor-liquid interface. Extra mass source M_{ml} was added at the bubble base in accordance with experimental data to simulate the evaporation of micro layer.

Fig. 1 presents a bubble in subcooled fluid, Q_{sd} is the energy released by bubble cap in subcooled domain, Q_{sl} stands for the energy absorbed by bubble cap in superheated liquid layer, Q_c is the total energy absorbed by bubble cap, Q_{ml} accounts for the evaporation energy of micro layer, Q_t stands for the total energy. And q is determined as heat flows, q_{sd}, q_{sl}, q_c, q_{ml} and q_t are calculated by temporal differentiation of Q_{sd}, Q_{sl}, Q_c, Q_{ml}, and Q_t respectively. The relationships of them are shown as follows:

$$Q_c = Q_{sl} - Q_{sd} \tag{1}$$

* Corresponding author.
E-mail address: pengch@ustc.edu.cn (C. Peng).

https://doi.org/10.1016/j.anucene.2018.10.005
0306-4549/

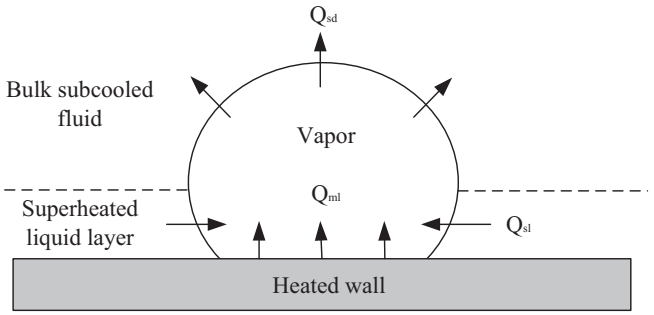

Fig. 1. Single bubble growth in the subcooled water.

$$Q_t = Q_{ml} + Q_c = Q_{ml} + Q_{sl} - Q_{sd} \tag{2}$$

2. Numerical simulation

2.1. Governing equations

The equations need to be solved in simulations are the conservation equations for mass, energy, momentum and volume fraction.

$$\nabla \cdot (\rho u) = \dot{\rho} \tag{3}$$

$$\frac{\partial \rho cT}{\partial T} + \nabla \cdot (u \cdot \rho cT) = \nabla \cdot (\lambda \cdot \nabla T) + h \tag{4}$$

$$\frac{\partial \rho \vec{u}}{\partial t} + \nabla (u \cdot \rho u) = -\nabla p + \nabla \cdot (\mu \cdot \nabla u) + S_s + S_g \tag{5}$$

$$\frac{\partial \alpha_l}{\partial t} + \nabla \cdot (u \cdot \alpha_l) = \frac{\dot{\rho}}{\rho} \alpha_l \tag{6}$$

The source term $\dot{\rho}$ on the right sides of Eqs. (3) and (6) is mass transfer in phase change process, and the source term h of Eq. (4) is energy change during the phase transition. The two volumetric forces S_s and S_g in Eq. (5) account for surface tension force and gravity respectively. The CSF (Continuum Surface Force) model proposed by Brackbill et al. (1992) has been implemented in VOF calculations. In CSF model, the surface tension can be written in terms of the pressure jump across the surface. The force at the surface can be expressed as a volume force using the divergence theorem. It has the following form:

$$S_s = \sigma \frac{\alpha_l \rho_l \kappa_v \nabla \alpha_v + \alpha_v \rho_v \kappa_l \nabla \alpha_l}{0.5(\rho_l + \rho_v)} \tag{7}$$

$$n_l = \nabla \alpha_l, n_v = \nabla \alpha_l \tag{8}$$

$$\vec{n} = \frac{n}{|n|} \tag{9}$$

$$\kappa_l = \nabla \cdot \vec{n}_l, \kappa_v = \nabla \cdot \vec{n}_v \tag{10}$$

Whereσrepresents surface tension coefficient, $\rho$is density, α stands for volume fraction in control volume n is the surface normal. The curvature,κ, is defined in terms of the divergence of unit normal $\vec{n}$. Subscripts l and v stand for liquid phase and vapor phase respectively. In the cells who contain two phases, physical properties such as density, dynamic viscosity and thermal conductivity can be calculated by average volume fraction.

2.2. Phase change model

The phase change model proposed by Lee (Lee and Veziroglu, 1980) was implemented in calculation and it can be written as Eqs. (11), (12) and (13), where T and T_{sat} are local temperature and local saturation temperature respectively. If T exceed T_{sat}, the evaporation occurs. Liquid phase would transfer into the vapor phase and the mass source can be written as:

$$M = c_l \alpha_l \rho_l \frac{T - T_{sat}}{T_{sat}} \tag{11}$$

If T is equal to T_{sat}, neither evaporation nor condensation would occur. Otherwise the condensation occurs. Vapor phase would change into liquid phase. And the mass is:

$$M = c_v \alpha_v \rho_v \frac{T - T_{sat}}{T_{sat}} \tag{12}$$

where c_l and c_v are the relaxation coefficients which can be modified artificially to control the phase change rate during the calculation. According to Wei and Pan (2011), the coefficients are set as 100 s^{-1} to keep the interface temperature around T_{sat}. After many attempts, $c_l = c_v = 800\ s^{-1}$ is adopted here. The energy absorbed/released during phase change, h, could be calculated by Eq. (13) where the h_{lv} is latent heat.

$$h = h_{lv} M \tag{13}$$

Assumed that the *iso*-line of 0.5 vol fraction is vapor-liquid interface, when evaporation or condensation occur, the mass sources are added at cells who are closed to interface but not exactly contain the interface. The mass sources of liquid and vapor have same value but adverse sign. Thus the interface can be kept from deformation during calculation and mass is conservative.

2.3. Micro layer

Micro layer is the thin liquid layer between the bubble and heating wall when bubble is growing up. Tiny thickness and drastic evaporation are two features of micro layer. Many researches has been done to investigate micro layer. Jung and Kim (2014) found that the thickness of micro layer is only about few micrometers by laser interferometry experiment. Yabuki and Nakabeppu (2014) deduced that about 50% of the total evaporation is contributed by micro layer during bubble growth by analyzing experiment results. Fig. 2 shows

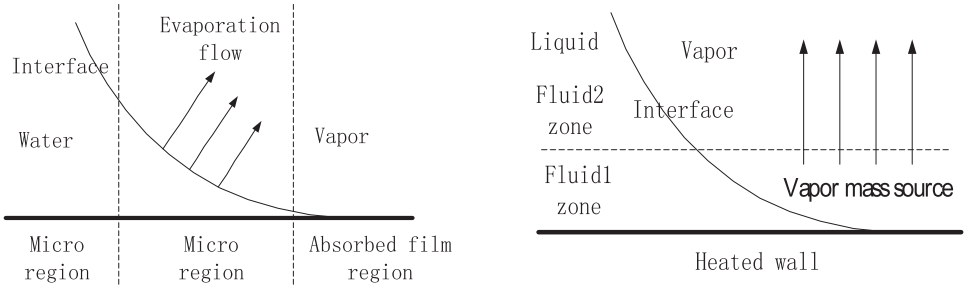

Figs. 2 and 3. Actual micro region evaporation (left) and a simplify method in simulation (right).

the actual evaporation at bubble base. As can be seen in the picture, the evaporation mainly lies in macro region and micro region, but not absorbed film region for liquid is almost dry out here. To simplify the calculation, a model shown in Fig. 3 has been adopted. In Fig. 3 the computational domain is divided into Fluid1 and Fluid2. Fluid1 is attached to the superheating wall and the thickness of Fluid1 is much smaller than bubble size. It's supposed that the thickness of Fluid1 is 0.24 mm for the convenience of dependency test. Specific vapor mass source $M_{ml} = f(t)$ corresponding to Ref. (Yabuki and Nakabeppu, 2016) was added to cells who contain vapor phase in Fluid1 to simulate the evaporation of micro layer.

2.4. Experiment & computational domain

Two experiments in Ref. (Yabuki and Nakabeppu, 2016) has been chosen as validation cases. The experiments recorded clear photographs of isolated bubble generation process in subcooled boiling water as shown in Figs. 4 and 5. Bubble contours, departure time and contact angle can be got from the photos. In the experiments, a MEMS (Micro-Electro-Mechanical System) sensor was put at the base to get temperature distribution, a high-speed camera was used to take photos. The schematic of experimental set-up is presented in Fig. 6. A glass cell (10 mm × 10 mm) was put on the MEMS sensor with a thin film heater attached to the bottom of the MEMS sensor. A tiny hydrogen bubble generated by electrolysis of the water was used to act as a bubble nucleus.

The computational domain consisted of solid domain (10 mm × 0.2 mm) and fluid domain (10 mm × 12.24 mm) is shown in Fig. 7. The fluid domain has been divided into Fluid1 (10 mm × 0.24 mm) and Fluid 2 (10 mm × 12 mm). The boundary between the two zones was interior and the top of the domain was pressure-outlet whose back-flow temperature was equal to subcooled bulk fluid. The left side and right side of the fluid domain were no-slip wall. The temperature of bottom substrate was set as 388.8 K in case A and 395.9 K in case B according to Ref. (Yabuki and Nakabeppu, 2016) with nucleation site at the middle of top surface, and it was presupposed that the temperature would not change during the process for the whole process only last few milliseconds. The temperature of bulk fluid in two cases was 363 K and 353.4 K respectively under 1 atmosphere. The physical properties of materials used in calculation are listed in Table 1.

To get the initial temperature field, assume that the q_c reaches maximum value when bubble height is equal to saturation temperature *iso*-line height. So it can be deduced from available data in

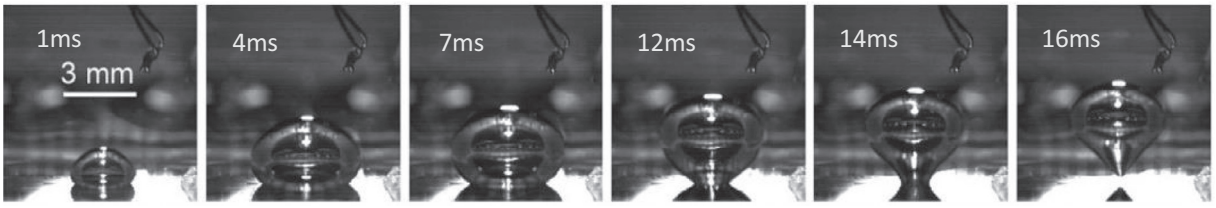

Fig. 4. The evolution of the bubble shape in case A.

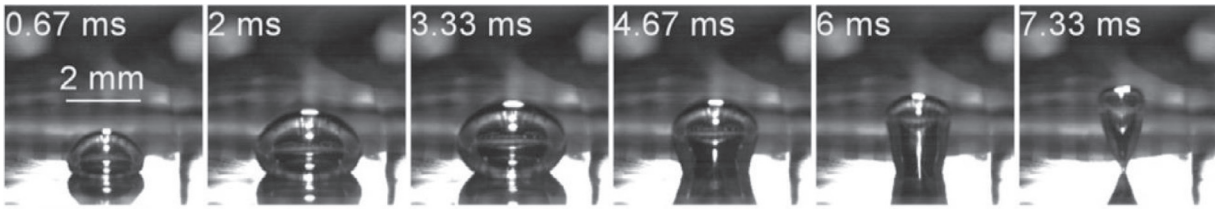

Fig. 5. The evolution of the bubble shape in case B.

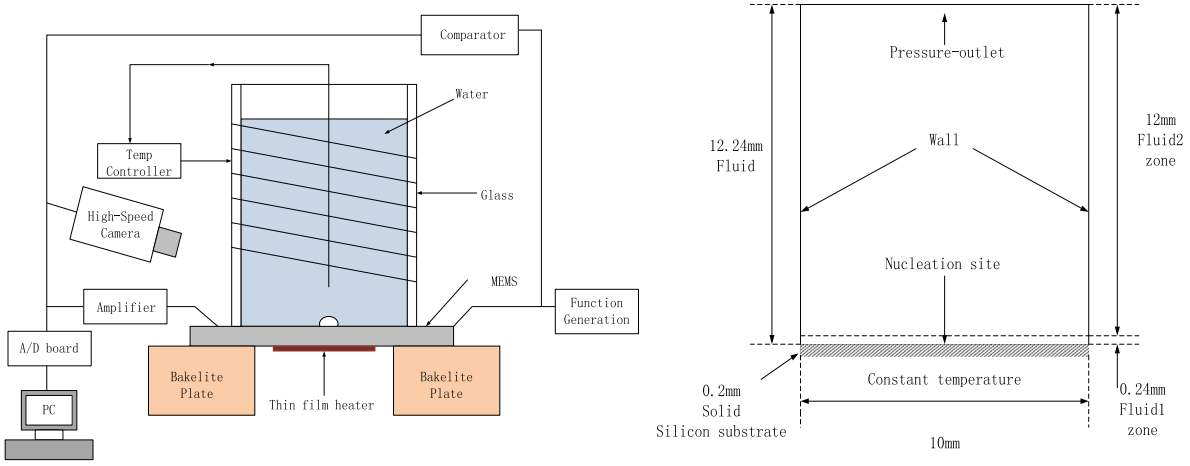

Figs. 6 and 7. The set-up of experiment (left). The schematic of computational domain (right).

Table 1
Physical properties of materials at atmospheric pressure.

	Vapor	Liquid	Silicon
Density (kg/m^3)	5.54×10^{-1}	9.982×10^{2}	2.33×10^{3}
Heat capacity (J/kg/K)	2.03×10^{3}	4.182×10^{3}	7.66×10^{2}
Thermal conductivity (W/m/K)	2.61×10^{-2}	6.0×10^{-1}	1.48×10^{2}
Viscosity (Pa·s)	1.34×10^{-5}	1.0×10^{-3}	
Latent heat (J/kg)	2.26×10^{6}		
Surface tension coefficient (N/m)	5.9×10^{-2}		

Ref. (Yabuki and Nakabeppu, 2016) that the *iso*-line of saturation temperature is at the height of about 1.7 mm and 1.2 mm in two cases respectively at initial stage. At first, the heating wall would heat the water. When the temperature at the height of 1.7 mm or 1.2 mm rose to 373 K, a hemispherical seed bubble whose radius was 0.2 mm would be put at nucleation site. This was an initial stage. Then the seed bubble would grow by evaporation in bubble cap and extra vapor source at bubble base whose temperature was pre-assumed as 388.8 K or 395.9 K which is equal to the temperature of heating wall. This method neglects the process of bubble growth up to the seed bubble radius and this may influence the accuracy of calculation at initial stage. So in the following passage, the first picture of simulation results has been omitted.

2.5. Computation settings

The VOF solver in ANSYS FLUENT was used for computation. The complete incompressible N-S equations were solved using PISO (Pressure-Implicit with Splitting of Operators) method. The momentum and energy equations were discretized using the second-order upwind scheme, and the equation of volume fraction by the Geo-Reconstruct scheme. The surface tension force was computed by the CSF model. The interface was reconstructed by PLIC (Piecewise Linear Interface Calculation) geometry restructuring method. The time step was set as 10^{-5} s to make sure that the Courant number was less than 0.1. At each time step the solution was assumed to converge when the normalized residual of energy equation was lower than 10^{-6} and the normalized residual of all other variables were lower than 10^{-4}.

Table 2
Computational grids of different sizes.

Grid	Δx(μm)	Δy(μm)	Cell amount
a	80	80	19,125
b	40	60	51,000
c	40	40	76,500
d	20	20	306,000

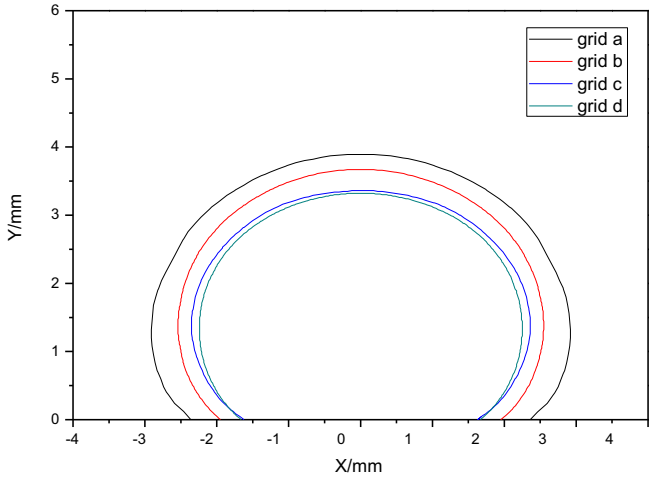

Fig. 8. Contours got by different grids at 7 ms.

In previous work, Lal et al. (2012) numerically studied subcooled nucleate pool boiling with finest 62.5 μm grid size. Jia et al. (2014) conducted numerical simulation of nucleate boiling at a constant surface temperature with the mesh size of 50 μm. The dependency of grid size has also been concerned here. Different sizes of grids ranging from 20 μm to 80 μm shown as Table 2 have been calculated in case A and the bubble contours at 7 ms were presented in Fig. 8. The thickness of Fluid1 (0.24 mm) can be divided by all these values with no remainder. Hence, the specific vapor mass source term can be applied easily. It's obvious that the results of grid c are very close to grid d while the calculation in grid d takes much longer time than that in grid c. Thus the grid scale was finally set as 40 μm×40 μm to save computation resource.

3. Results and discussion

3.1. Bubble contours

The bubble contours before bubble departure are shown in Figs. 9–11. Each picture scale corresponds to 6 mm × 6 mm in the following text. It can be observed that the bubble changes from a hemisphere to an ellipsoid and eventually becomes a pear shape in both cases. The change trend of bubble shape is similar to that in Figs. 4 and 5. The maximum lateral diameter and height of bubble got by computation have been compared with experimental data in Fig. 12. Obviously, in two cases the lateral diameter rises at first then decreases while the height is always increasing. In case A the computational results fit well with experimental data, but in case B the bubble height got by simulation is smaller than that in photograph.

3.2. Heat flow

Much attention should be paid to the heat flow distribution for it determined the bubble generation. Fig. 13 shows that the variations of q_t, q_{ml} and q_c in two cases have a similar tendency. At first the q_{ml} increases due to the extension of the bubble base and micro region, then it decreases for the shrinkage of contact area and the expansion of absorbed film region until the bubble departure. At initial stage, q_c has positive value for most of the bubble was immersed in superheated liquid layer, then more bubble cap was exposed to subcooled water with the growth of the bubble and q_c became negative. The q_t is the sum of q_{ml} and q_c, and they can be integrated to get Q_t, Q_{ml} and Q_c respectively.

3.3. Temperature and velocity fields

Figs. 14 and 15 present the temperature fields at different times which cannot be got by experiment directly. The temperature of extra vapor added at bubble base is pre-assumed as 388.8 K and 395.9 K, so the vapor temperature inside the bubble is higher than saturation temperature. But the liquid-vapor interface is almost kept at saturation temperature for the mass change is occurring there. The energy absorbed/released by phase change process can keep the temperature stable. During the whole process, the wall temperature is assumed to be constant because the time is very short, despite there is a wall temperature decrease in Ref. (Yabuki and Nakabeppu, 2016).

Figs. 16 and 17 show the velocity fields in two cases. At initial stage, the direction of velocity is directed from the inside of the bubble to the outside of the bubble for bubble is growing

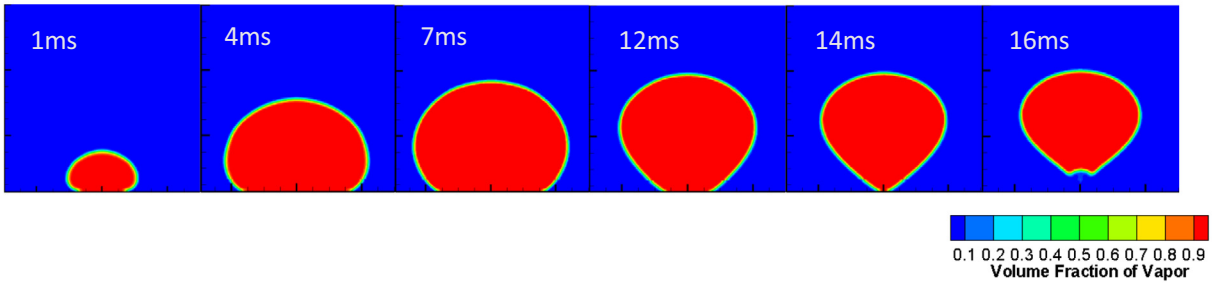

Fig. 9. The evolution of bubble contours in case A.

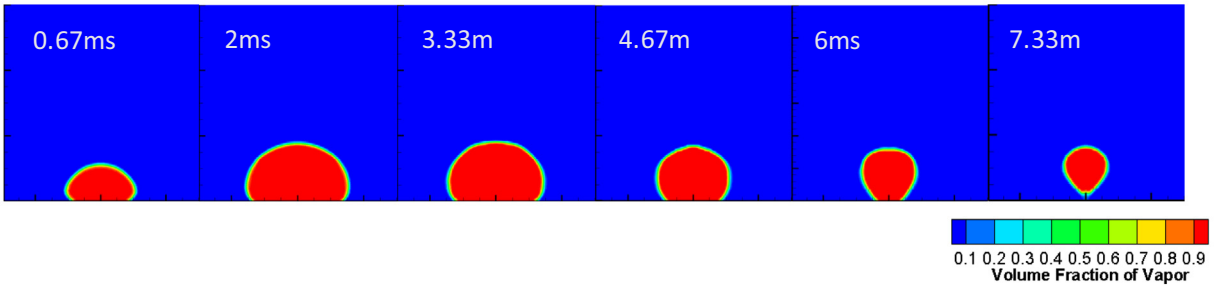

Fig. 10. The evolution of bubble contours in case B.

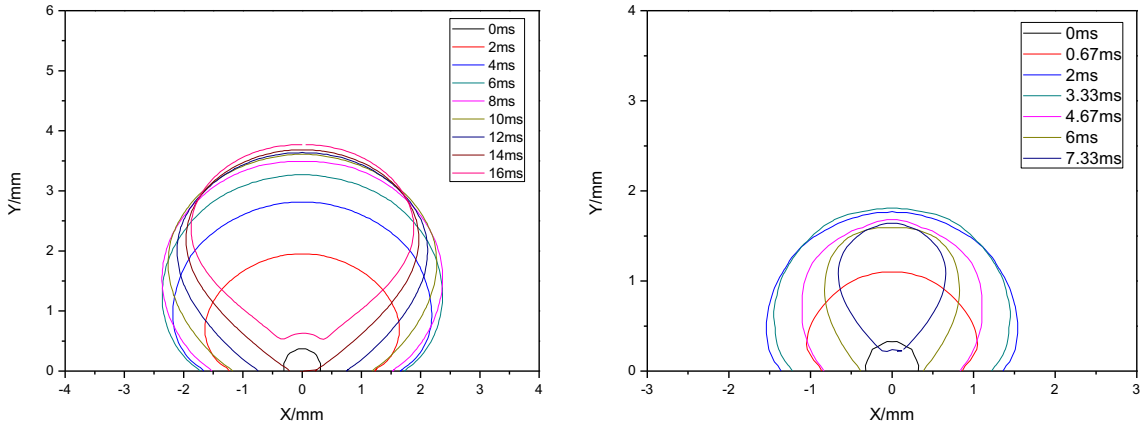

Fig. 11. The bubble contours in case A (left) and case B (right).

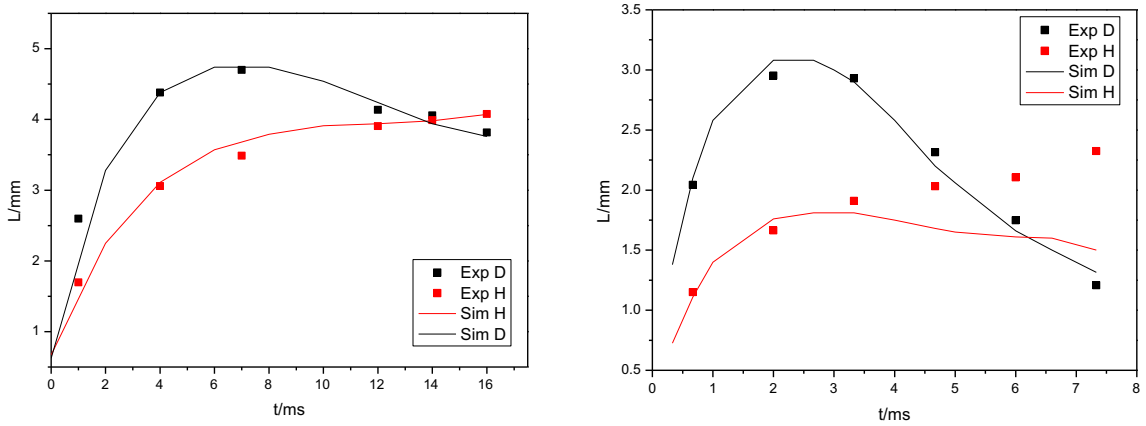

Fig. 12. Lateral diameters and bubble heights in case A (left) and case B (right).

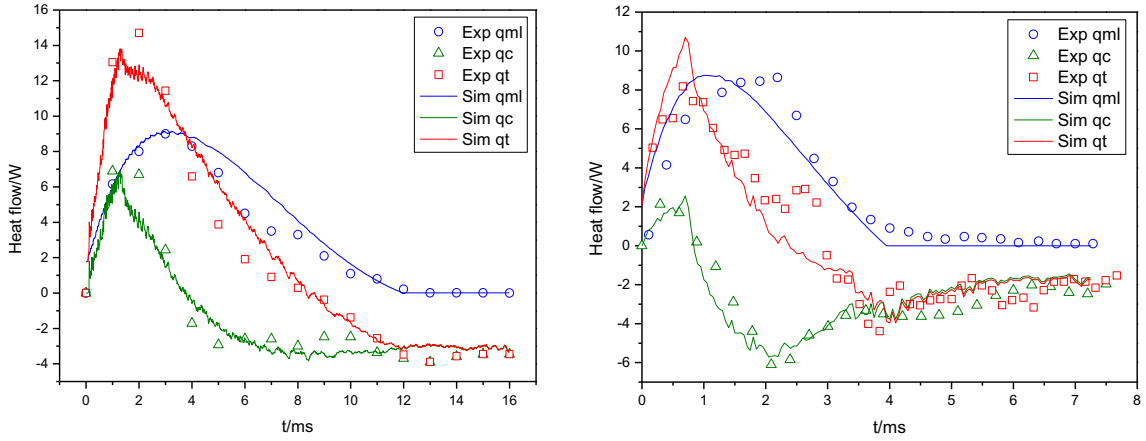

Fig. 13. The comparison of q_{ml}, q_c and q_t got by simulation and experiment in case A (left) and case B (right).

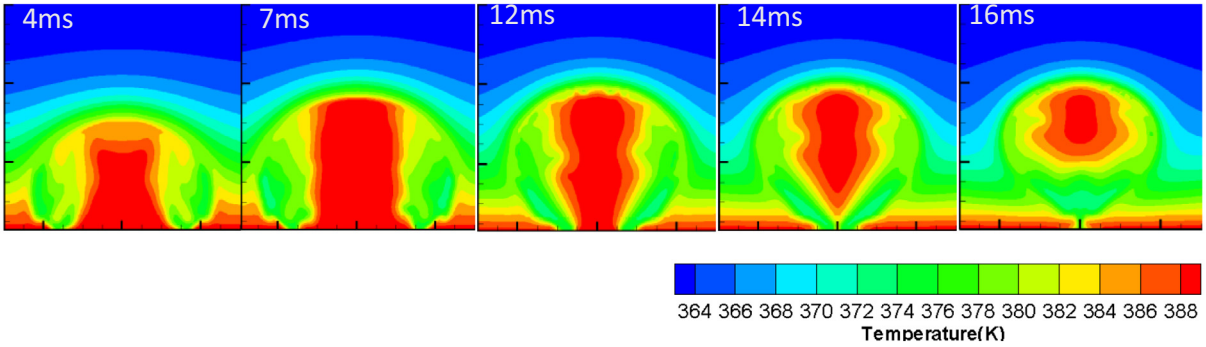

Fig. 14. The temperature fields at different times in case A.

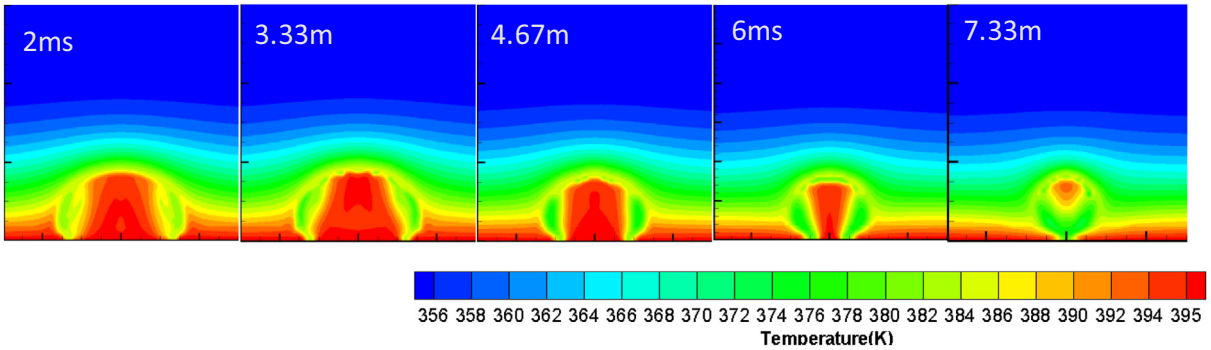

Fig. 15. The temperature fields at different times in case B.

dramatically in the period. Then two vortexes occur inside the bubble attached to interface on the left and right side. Because the newly produced steam from the bottom of the bubble flows vertically upwards in the center of the bubble. When the steam encounters the vapor-liquid interface, part of the steam will liquefy due to condensation. The remaining part of the steam changes flow direction and flows down along the vapor-liquid interface. But when it comes to new steam generated by the interface who are submerged in superheated layer, it will change direction again and flows toward bubble center with newly generated steam. Thus, it looks like that there are vortexes in the middle part of both sides of the bubble.

3.4. Mass transfer

Mass transfer is the most important issue in calculation. Figs. 18 and 19 present the distribution of vapor mass source comparing with bubble contour in two cases. As can be seen, there are obvious evaporation occurring at the bottom of the bubble cap and obvious condensation occurring at the top bubble cap in initial period. With time goes by, the degree of evaporation and condensation both decrease for the energy absorbed/released makes the temperature closer to saturation temperature at the interface. Finally the evaporation and condensation are greatly diminished when bubble is detached.

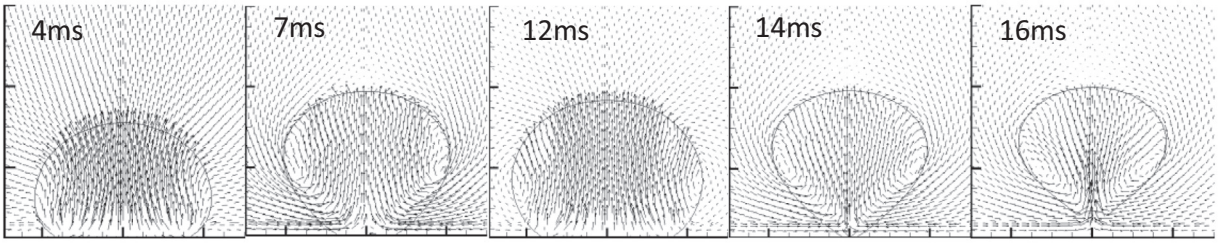

Fig. 16. The velocity fields at different times in case A.

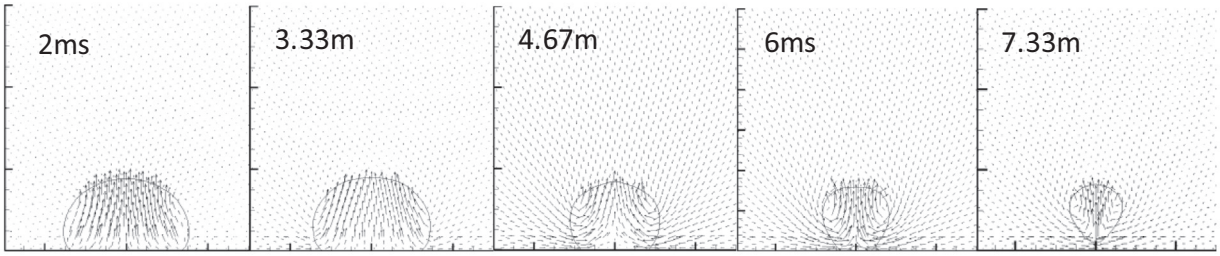

Fig. 17. The velocity fields at different times in case B.

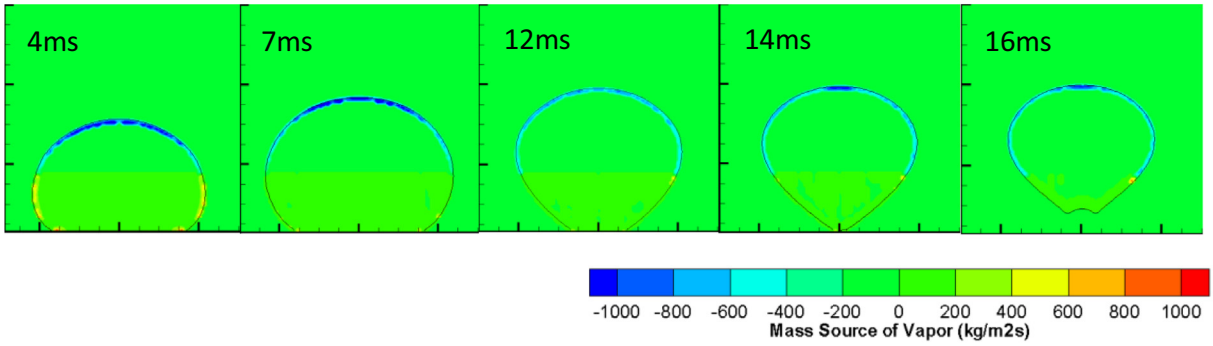

Fig. 18. Distribution of vapor mass source at different times in case A.

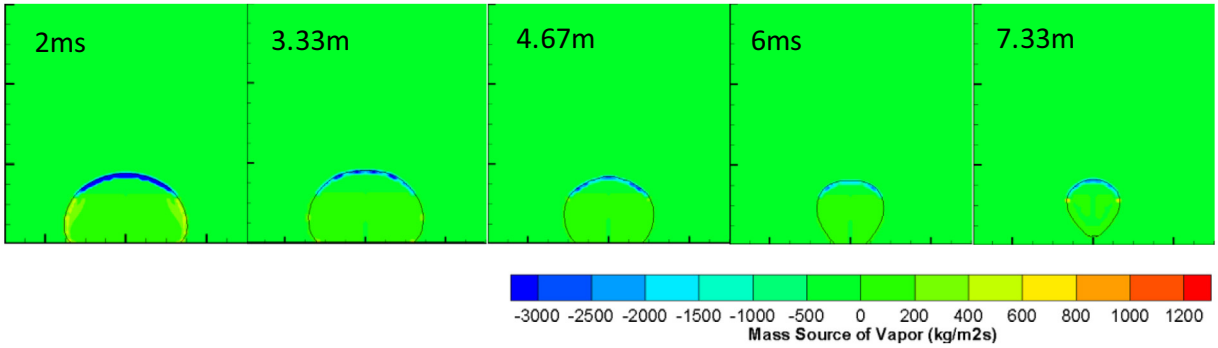

Fig. 19. Distribution of vapor mass source at different times in case B.

It can also be observed that the mass source was located on cells who are closed to interface but not exactly at interface. This modification can keep the liquid-vapor interface sharp and clear during the calculation, despite it may cause errors in the flow velocity, pressure and temperature distributions. In flow boiling case and saturated boiling case, this adjustment can also get results close to the experiment. But FLUENT cannot get a satisfactory outcome under 3-D condition, because the geometry reconstruction scheme for moving surface under 3-D condition in FLUENT is not mature enough. So there is still a lot of work to be done.

4. Conclusions

Present research is an investigation of numerical tool for the subcooled nucleate boiling. The method can be used to forecast further experimental case. In this paper two cases of a single bubble generation in subcooled boiling has been numerically investigated and the simulation results fit well with the experimental data. Some conclusions can be drawn from this work:

1. Based on experimental temperature results and micro layer source data, present method can obtain reasonable bubble growth procedure in subcooled fluid under 2-D condition.
2. During the bubble growth process, the bubble changes from a hemisphere to an ellipsoid and eventually becomes a pear shape. The lateral diameter rises at first then decreases while the height is always increasing. Within the bubble the vapor rises in the center and flows down along the bubble surface. The velocity of fluid would change direction at the interface and there are two vortexes on the left and right side in the middle part of the bubble.
3. The redistribution of mass source term at interface can avoid the deformation of bubble shape and keep the liquid-vapor interface sharp and clear during the calculation.

The method adopted in this paper strongly relies on experiment data such as heat flow in micro layer, wall temperature and so on. Many efforts should be done to get over the dependences in future research. In addition, we are running visual experiment on bubble growth and motion in rectangular channel with different subcooling levels and flow states, the experiment data would be used to verify and improve the existing method to fulfill the demand of engineering design.

Acknowledgments

This work was financially supported by the National Key R&D Program of China (Grant No. 2017YFE0300604), and also supported by National Natural Science Foundation of China (Grant No. 11305169).

References

Brackbill, J.U., Kothe, D.B., Zemach, C., 1992. A continuum method for modeling surface tension. J. Comput. Phys. 335–354.
Hardt, S., Wondra, F., 2008. Evaporation model for interfacial flows based on a continuum-field representation of the source terms. J. Comput. Phys. 227, 5871–5895.
Jia, H.W., Zhang, P., Fu, X., Jiang, S.C., 2014. A numerical investigation of nucleate boiling at a constant surface temperature. Appl. Therm. Eng., 1–10
Jung, S., Kim, H., 2014. An experimental method to simultaneously measure the dynamics and heat transfer associated with a single bubble during nucleate boiling on a horizontal surface. Int. J. Heat Mass Transf. 73, 365–375.
Lal, S., Sato, Y., Niceno, B., 2012. Direct numerical simulation of subcooled nucleate pool boiling. Int. J. Math., Comput., Phys., Electr. Comput. Eng. 6 (3).
Lee, W.H.A., 1980. Pressure iteration scheme for two-phase flow modeling. In: Veziroglu, T.N. (Ed.), Multiphase transport fundamentals, Reactor Safety, Applications. Hemisphere Publishing, Washington, D.C..
Tomar, G., Biswas, G., Sharma, A., Agrawal, A., 2005. Numerical simulation of bubble growth in film boiling using a coupled level-set and volume-of-fluid method. Phys. Fluids 17, 112103.
Wei, J.H., Pan, L.M., et al., 2011. Numerical simulation of bubble behaviors in subcooled flow boiling under swing motion. Nucl. Eng. Des. 241, 2898–2908.
Welch, S.W.J., Wilson, J., 2000. A volume of fluid based method for fluid flows with phase change. J. Comput. Phys. 160, 662–682.
Yabuki, T., Nakabeppu, O., 2014. Heat transfer mechanisms in isolated bubble boiling of water observed with MEMS sensor. Int. J. Heat Mass Transf. 76, 286–297.
Yabuki, T., Nakabeppu, O., 2016. Microscale wall heat transfer and bubble growth in single bubble subcooled boiling of water. Int. J. Heat Mass Transf., 851–860